POLITECNICO DI TORINO
Repository ISTITUZIONALE

A Novel Tri-State DC–DC Converter and Robust Nonlinear Control for Fuel Cell–Ultra Capacitor based Hybrid Electric Vehicles

Original
A Novel Tri-State DC–DC Converter and Robust Nonlinear Control for Fuel Cell–Ultra Capacitor based Hybrid Electric Vehicles / Khan, A., Ahmad, I., Ahmed, S., Alatawi, K.S., Almasoudi, F.M., Zeb, K., Neamah, H.A.. - In: RESULTS IN ENGINEERING. - ISSN 2590-1230. - STAMPA. - 30:https://doi.org/10.1016/j.rineng.2026.111696(2026), pp. 1-23. [10.1016/j.rineng.2026.111696]

Availability:
This version is available at: 11583/3012433 since: 2026-06-25T13:53:28Z

Publisher:
Elsevier

Published
DOI:10.1016/j.rineng.2026.111696

Terms of use:

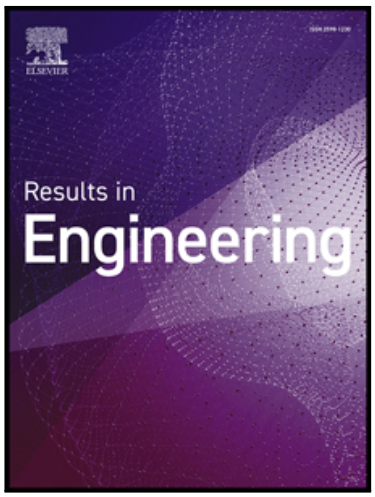
This article is made available under terms and conditions as specified in the corresponding bibliographic description in the repository

Publisher copyright

(Article begins on next page)

21 November 2026

Journal Pre-proof



A Novel Tri-State DC–DC Converter and Robust Nonlinear Control for Fuel Cell–Ultra Capacitor based Hybrid Electric Vehicles

Adnan Khan, Iftikhar Ahmad, Shahzad Ahmed, Khaled S. Alatawi, Fahad M. Almasoudi, Kamran Zeb, Husam A. Neamah

PII: S2590-1230(26)02720-9
DOI: https://doi.org/10.1016/j.rineng.2026.111696
Reference: RINENG 111696

To appear in: *Results in Engineering*

Received date: 10 March 2026
Revised date: 4 June 2026
Accepted date: 22 June 2026

Please cite this article as: Adnan Khan, Iftikhar Ahmad, Shahzad Ahmed, Khaled S. Alatawi, Fahad M. Almasoudi, Kamran Zeb, Husam A. Neamah, A Novel Tri-State DC–DC Converter and Robust Nonlinear Control for Fuel Cell–Ultra Capacitor based Hybrid Electric Vehicles, *Results in Engineering* (2025), doi: https://doi.org/10.1016/j.rineng.2026.111696

This is a PDF of an article that has undergone enhancements after acceptance, such as the addition of a cover page and metadata, and formatting for readability. This version will undergo additional copyediting, typesetting and review before it is published in its final form. As such, this version is no longer the Accepted Manuscript, but it is not yet the definitive Version of Record; we are providing this early version to give early visibility of the article. Please note that Elsevier's sharing policy for the Published Journal Article applies to this version, see: https://www.elsevier.com/about/policies-and-standards/sharing#4-published-journal-article. Please also note that, during the production process, errors may be discovered which could affect the content, and all legal disclaimers that apply to the journal pertain.

© 2026 Published by Elsevier B.V.
This is an open access article under the CC BY-NC-ND license (http://creativecommons.org/licenses/by-nc-nd/4.0/)

Journal Pre-proof

HIGHLIGHTS

- An FC–UC-based HESS employing tri-state boost and tri-state buck–boost converters is developed for HEV applications. The proposed converters eliminate the RHP zero CCM, thereby avoiding non-minimum phase behavior and improving transient response characteristics.
- Lyapunov redesign, SMC, and ST-SMC are formulated for DC-bus voltage regulation and coordinated FC–UC current control.
- A Lyapunov-based stability framework is established to prove the global asymptotic stability of the closed-loop HESS under the proposed control laws.
- Simulation and HIL validation using a TMS320F28379D dual-core microcontroller confirms the effectiveness of the proposed control framework, with ST-SMC outperforming Lyapunov redesign and conventional SMC.

Journal Pre-proof

Journal Pre-proof

A Novel Tri-State DC–DC Converter and Robust Nonlinear Control for Fuel Cell–Ultra Capacitor based Hybrid Electric Vehicles

Adnan Khan, Iftikhar Ahmad, Shahzad Ahmed, Khaled S. Alatawi, Fahad M. Almasoudi, Kamran Zeb, and Husam A. Neamah*

Abstract

Conventional DC–DC power converters employed in electric vehicle (EV) applications, including boost, buck-boost, fly-back, and interleaved converters, exhibit a right-half-plane (RHP) zero under continuous conduction mode (CCM), resulting in non-minimum-phase behavior and degraded dynamic performance. This research proposes a novel hybrid energy storage system (HESS) based on tri-state boost and tri-state buck-boost converters that eliminate the RHP zero, thereby enabling faster transient response and improved controllability. To achieve precise regulation of the system, three nonlinear control strategies, namely Lyapunov redesign, sliding mode control (SMC), and super-twisting sliding mode control (ST-SMC), are developed for accurate DC-bus voltage regulation and precise tracking of the polymer electrolyte membrane fuel cell (PEMFC) and ultra-capacitor (UC) currents. A rigorous Lyapunov-based stability analysis is presented to establish the global asymptotic stability of the closed-loop system. The proposed controllers are validated through MATLAB/Simulink simulations under the European Extra Urban Driving Cycle (EUDC) and hardware-in-the-loop (HIL) implementation using a TMS320F28379D dual-core microcontroller platform. Comparative results demonstrate that the ST-SMC achieves superior dynamic performance with reduced tracking error, minimized overshoot/undershoot, improved disturbance rejection capability, reduced chattering, and the lowest integration of square error (ISE) value of 1.689×10^4 compared with the Lyapunov redesign and SMC approaches. Furthermore, the close agreement between simulation and HIL results confirms the practical feasibility, robustness, and real-time applicability of the proposed control framework for EV powertrain applications.

Index Terms

Tri-state boost converter, Tri-state buck-boost converter, right half-plane, sliding-mode control (SMC), super-twisting sliding-mode control (ST-SMC), and hybrid energy storage system (HESS).

I. Introduction

Traditional vehicles rely heavily on the consumption of substantial amounts of gasoline, diesel, and other fossil fuels, contributing to the depletion of global reserves, while struggling with increasing daily prices [1], [2]. The use of these fuels also results in the emission of a substantial amount of carbon dioxide (CO_2), a greenhouse gas known for its contribution to global warming [3]. Consequently, the world's climate is undergoing rapid changes. With the increasing use of conventional vehicles, the demand for energy is also increasing, which requires the exploration of alternative solutions [4], [5]. The proposed solution is the replacement of conventional vehicles with EVs [6]. EVs can be fully or partially powered by electric energy, offering the advantages of significantly lower operational costs and a reduced environmental footprint due to their minimal or zero dependence on fossil fuels.

The history of EVs dates back to the early nineteenth century when inventors began to experiment with the conversion of automobiles to EVs [7]. EVs come in various forms, including hybrid EVs (HEVs), plug-in hybrid EVs (PHEVs), battery-based EVs (BEVs), and fuel cell-based hybrid EVs (FHEVs), each with its unique set of advantages and disadvantages. HEVs and PHEVs operate using both an electric motor and an internal combustion engine (ICE), making them not entirely emission-free. PHEVs, in particular, require an external charging source, which is efficient but requires access to fast charging stations. BEVs produce zero emissions, but often have limited driving ranges. FHEVs, while they address some of these concerns, tend to be slightly more expensive compared to other EV topologies [8]. The configuration of the FHEV is illustrated in Fig.2. Previously, various HEV topologies, including parallel, series, and propulsion hybrid EVs, were discussed in detail in [9].

Most fuel cell-based hybrid electric vehicles (FHEVs) typically incorporate two energy storage units: a primary storage unit (PSU) with a higher energy capacity and an auxiliary storage unit (AEU) designed for quick power delivery, enabling smooth

Adnan Khan (adnan.khan@polito.it) is with the Department of Energy, Politecnico di Torino (Polito), Corso Duca degli Abruzzi, 24,10129 Torino, Italy.

Iftikhar Ahmad (iftikhar.rana@seecs.edu.pk), and Shahzad Ahmed (shahmed.msee18seecs@seecs.edu.pk) are with the School of Electrical Engineering and Computer Science, National University of Sciences and Technology (NUST), Islamabad, Pakistan.

Khaled S. Alatawi (khaled@ut.edu.sa) and Fahad M. Almasoudi (falmasoudi@ut.edu.sa) are with the Electrical Engineering Department, Faculty of Engineering, University of Tabuk, Tabuk 47913, Saudi Arabia.

Kamran Zeb (kamran.zeb@kfupm.edu.sa) is with the Interdisciplinary Research Center for Sustainable Energy Systems, King Fahd University of Petroleum and Minerals (KFUPM), Dhahran 31261, Saudi Arabia.

*Corresponding author: Husam A. Neamah (husam@eng.unideb.hu), Department of Electrical Engineering and Mechatronics, Faculty of Engineering, University of Debrecen, Debrecen, Hungary.

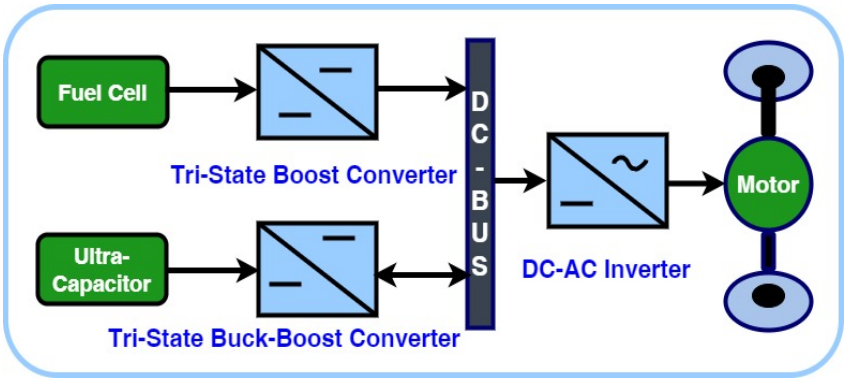


Fig. 1: Block diagram of HESS

and bidirectional transitions within the system. The PSU primarily offers an extended driving range, while the AEU assists in acceleration and regenerative braking [10]. In this context, the FC can serve as the PSU because of its high energy density, while the UC can function as the AEU, providing instantaneous power when needed. FCs possess a high energy density but lower power density and cannot solely meet the vehicle's power demands. Therefore, various combinations of AEU are used alongside the PSU, with the UC helping the FC during the acceleration and deceleration phases.

FCs are categorized into different types based on their performance characteristics, with the PEMFC commonly used in EVs due to its high energy density, lightweight nature and suitability for low temperature operation [11], [12]. The FC continuously supplies power to the traction motor during the vehicle's operation, provided there is a hydrogen supply. For transient activities such as starting, accelerating, and braking, the UC complements the PSU. The UC is recharged during downhill movement and during braking. DC bus accumulates energy from both the FC and the UC. Most EVs employ AC induction motors for traction, necessitating the use of an inverter before the traction motor to convert the DC bus voltage into AC voltage [13].

DC-DC power converters are crucial for efficient voltage regulation and effectively facilitate the interconnection of different energy sources with asynchronous motors. Various power converter topologies and control techniques, such as back-stepping and integral back-stepping Sliding Mode Control (SMC), an adaptive terminal SMC, and double-integral SMC suitable for EVs HESS are discussed in [14]–[27]. Additionally, [28]–[30] discuss bi-directional DC-DC power converters, flyback power converters, and multi-device interleaved DC-DC power converters, respectively. However, despite the extensive literature on Hybrid Energy Storage System (HESS) converter topologies and control techniques, limited attention has been given to the control of tri-state converters in FC and UC, particularly regarding their dynamic characteristics and closed-loop stability analysis. In conventional boost and buck-boost converters operating under CCM, the presence of the RHP zero introduces inverse response characteristics and bandwidth limitations, which degrade transient performance and complicate controller design [31]–[33]. These limitations complicate the controller design and reduce the dynamic performance of the overall HESS. In contrast, the proposed tri-state converter topology eliminates the RHP zero, thereby avoiding non-minimum phase behavior and enabling faster dynamic response, improved controllability, reduced overshoot and undershoot, and enhanced voltage regulation performance. This characteristic is particularly advantageous in EV applications where rapid power flow variations occur during acceleration, deceleration, and regenerative braking operations [33]. The visual representation in Fig.1 elucidates the fundamental setup of a HESS based on a Hydrogen FC and UC. The analytical methodologies used for the study of FC and UC based HESS predominantly embrace linear approaches, ensuring a focus on local stability. However, it is important to note that most DC-DC power converters are highly non-linear, and traditional linear controllers often fall short in meeting the performance requirements.

Although several nonlinear control strategies have been reported for HESS applications, many existing studies rely mainly on simulation-based validation without providing rigorous theoretical guarantees regarding closed-loop stability. In contrast to the existing studies, this work develops nonlinear controllers supported by rigorous Lyapunov-based global asymptotic stability analysis, thereby strengthening the theoretical foundation and robustness of the proposed control framework. Moreover, the proposed control strategies are specifically designed for tri-state converter-based FC-UC HESS, enabling improved transient performance and enhanced robustness against system uncertainties and disturbances. The main contributions of this paper are summarized as follows:

The main contributions of this paper are summarized as follows:

The structure of this paper is organized as follows.

Section II: discusses HESS and its significance in the context of EVs. Section III: presents the mathematical modeling of the HESS, providing a foundation for the subsequent control design. Section IV: Covers the design and analysis of controllers for the HESS, including the application of nonlinear control techniques. Section V: includes simulation results of the proposed controllers. These results are obtained through MATLAB/Simulink simulations and HIL testing using the TMS320F28379D

Journal Pre-proof

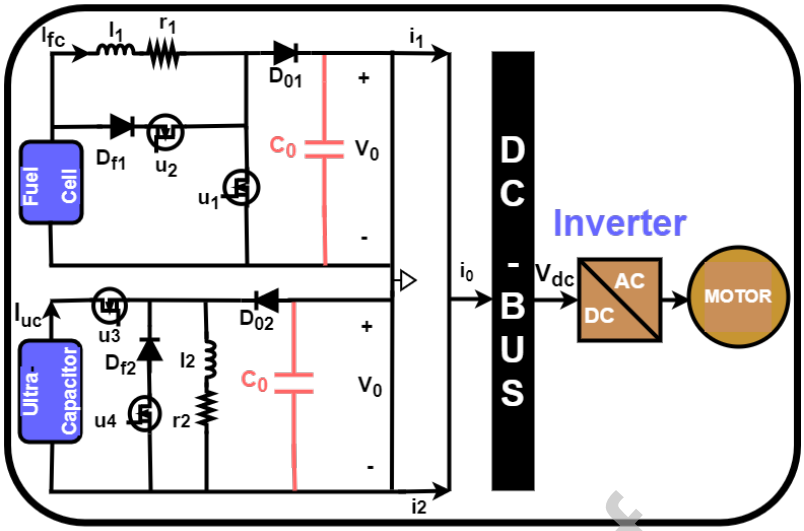


Fig. 2: Hybrid Electric vehicle schematic

dual-core microcontroller. Section VI: Offers conclusions drawn from the research and outlines potential avenues for future work in this area.

II. Hybrid Energy Storage System

In this section, the focus shifts to the HESS designed exclusively for EVs. Successful HESS for EVs must meet specific criteria such as high power density, extended service life, improved efficiency, and cost-effectiveness. The proposed HESS draws its power from two primary sources: a FC and an UC. Notably, the FC serves as a non-rechargeable energy source, while the UC can be recharged as needed. The HESS design aims to encompass all the essential characteristics required for an ideal HESS. The visual representations are given in Figs.1 and 2 in this section. Further details on the operation and features of the FC, UC, and Energy Management System (EMS) are elaborated below.

A. Fuel Cell

Within the HESS, the fundamental energy storage component is the FC. This component operates by generating energy through a chemical reaction that involves hydrogen and oxygen in the presence of an electrolyte. To connect the FC to the bus voltage, a Tri-state boost converter is employed. The selection of the FC is based on its ability to produce pure energy, which makes it a suitable choice for this application.

B. Ultra-capacitor

The UC boasts a high capacitance value and operates with two sizable parallel plates separated by a short distance. This design enables it to store a substantial amount of energy. UCs are characterized by their compact size, durability, and lightweight nature. They excel in delivering instant power to loads precisely when it is needed. To connect the UC to the DC-bus voltage, a Tri-state buck-boost converter is employed as part of the system design.

C. Planning for management of energy

Effective energy management planning is crucial for FHEVs, especially when the system is powered by multiple sources. The proposed system in this context is driven by two distinct energy sources. As illustrated in Fig.3, the energy storage system plays an essential role in the storage of regenerative energy and surplus energy, which is subsequently supplied to the system to meet various load conditions. The key operational scenarios are summarized below.

- Negative load: In instances of negative load, the FC remains inactive, while the UC is engaged in charging and recovering regenerative energy.
- Start up: During the initial phase where peak power demands are present, the UC is responsible for providing power since it can provide instant power, whereas the FC is unable to deliver peak power immediately.
- Light load: When the load is relatively light, the FC delivers consistent power output, with any excess power used by the UC for recharging.

Journal Pre-proof

Journal Pre-proof

- Heavy load: In situations that require a substantial amount of power, both the FC and UC work in tandem to provide the required power output.

This energy management strategy ensures the efficient utilization of energy sources based on the specific load conditions, optimizing the overall performance of the system.

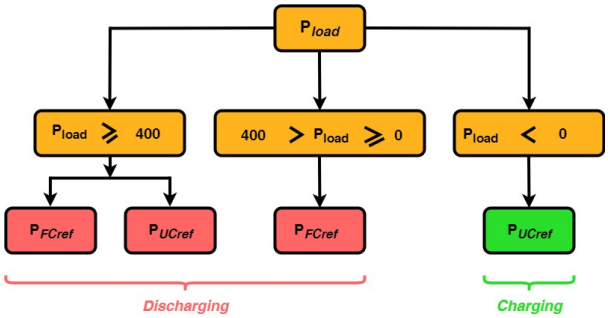


Fig. 3: Energy management strategy

III. Mathematical modeling of the system

This section delve into the mathematical modeling of the system. The dynamical Eqs. of the system essentially form the mathematical model, providing a foundation for the effective planning of the control and management strategies to ensure the efficient operation of the vehicle.

A. Boost converter modeling (FC)

The unidirectional Tri-state boost converter serves as the link between the FC and the DC-bus. It plays a crucial role in preventing the reverse voltage from reaching the FC source, which could potentially damage it. The schematic of this Tri-state boost converter is depicted in Fig.2. It consists of several components, including a high-frequency inductor l_1 with non-linearity r_1, two IGBT switches (main switch u_1 and freewheeling switch u_2), two diodes (D_{01} and freewheeling diode D_{f1}), and an output capacitor c. This converter operates in three distinct states: the boosting state $u_1 T_{sw}$, the capacitor charging state $\frac{(1-u1)}{2} T_{sw}$, and the free-wheeling state $\frac{(1-u1)}{2} T_{sw}$. It should be noted that $u_1 + \frac{(1-u1)}{2} + \frac{(1-u1)}{2} = 1$. Several control strategies can be used for this converter, with one straightforward approach being to fix the diode D_{01} interval while varying the intervals of the switches u_1 and u_2. The maximum gain is achieved when the freewheeling interval is equal to zero [31]. After applying volt-second balance and charge-second balance principles to the Tri-state boost converter, as shown in Fig.2, the following dynamical Eqs. are derived:

$$\frac{dI_{fc}}{dt} = u_1 \frac{(V_{fc} + V_{dc})}{2l_1} + \frac{V_{fc}}{2l_1} - \frac{V_{dc}}{2l_1} - \frac{r_1 I_{fc}}{l_1} \tag{1}$$

$$\frac{dV_{dc}}{dt} = (1 - u_1)\frac{I_{fc}}{2c} - \frac{i_1}{c} \tag{2}$$

I_{fc} represents the current from the FC. i_1 represents the output current of the Tri-state boost converter. V_{fc} corresponds to the source voltage of the FC. V_{dc} stands for the output voltage of the system.

B. Tri-state buck-boost converter modeling (UC)

The UC is connected to the system through a bidirectional Tri-state buck-boost converter, as shown in Fig.2. This converter consists of several components:

- Inductor l_2 with internal resistance r_2.
- Two IGBT switches, u_3, and u_4.
- Diode D_{02} for rectification.
- Freewheeling diode D_{f2}.

The Tri-state buck-boost converter operates in three distinct intervals: 1) Buck-Boost Interval: During this interval, u_3 is ON, D_{02} is reverse biased, and u_4 is OFF. Depending on the duty ratio of the switch u_3 relative to that of the diode D_{02}, the converter functions as a boost or buck converter. The specific mode (boost or buck) depends on the duty cycle of the switches. 2) Capacitor Charging Interval: In this interval, D_{02} is forward biased, while both u_3 and u_4 are in the OFF state. 3) Freewheeling interval: During this interval, D_{f2} is ON, while both u_3 and D_{02} are in the OFF state. The primary objective is to ensure that the UC current (I_{uc}) closely tracks its reference value provided by the energy management system. This control process

Journal Pre-proof

ensures efficient utilization of the UC's energy storage capabilities.
After applying the volt-second balance and charge-second balance principles to the Tri-state buck-boost converter depicted in Fig.2, the result is the following dynamical Eqs.: Eq. (3) represents the dynamic Eq. for the UC current (I_{uc}):

$$\frac{dI_{uc}}{dt} = u_{34}\frac{(2V_{uc} + V_{dc})}{2l_2} - \frac{V_{dc}}{2l_2} - \frac{r_2 I_{uc}}{l_2} \tag{3}$$

In this Eq., I_{uc} signifies the UC current, V_{uc} represents the UC voltage, and $V_{dc}$is the DC-bus voltage. Furthermore, u_{34} is a virtual control input. Eq. (4) depicts the dynamic Eq. for the output current of the Tri-state buck-boost converter (i_2)):

$$i_2 = (1 - u_{34})\frac{I_{uc}}{2c} - \frac{i_2}{c} \tag{4}$$

In this Eq., i_2) denotes the output current of the converter, I_{uc}) is the UC current, and c) represents the output capacitor associated with the converter. The input of the virtual control u_{34} influences the dynamics of these Eqs. These Eqs. govern the behavior of the UC system within the Tri-state buck-boost converter, taking into account the control input u_{34}, UC voltage (V_{uc}), UC current (I_{uc}), and DC-bus voltage (V_{dc}).

C. Global system modeling

The combination of Eqs. (1) to (4) results in the following global system modeling Eqs.:

$$\frac{dI_{fc}}{dt} = u_1\frac{(V_{fc} + V_{dc})}{2l_1} + \frac{V_{fc}}{2l_1} - \frac{V_{dc}}{2l_1} - \frac{r_1 I_{fc}}{l_1} \tag{5}$$

$$\frac{dI_{uc}}{dt} = u_{34}\frac{(2V_{uc} + V_{dc})}{2l_2} - \frac{V_{dc}}{2l_2} - \frac{r_2 I_{uc}}{l_2} \tag{6}$$

$$\frac{dV_{dc}}{dt} = (1 - u_1)\frac{I_{fc}}{2c} + (1 - u_{34})\frac{I_{uc}}{2c} - \frac{i_0}{c} \tag{7}$$

These Eqs. describe the dynamic behavior of the entire system, including the FC, UC and the DC-bus voltage, taking into account the control inputs u_1 and u_{34}. These dynamics are crucial for designing a controller to regulate and optimize the system's performance. To design a controller for the dynamics described by Eqs. (5) to (7), the proposed derived average model for one switching period is as follows:
Eq. (8): Describes the average dynamics of the FC current (X_1):

$$\dot{X}_1 = \mu_1\frac{(V_{fc} + X_3)}{2l_1} + \frac{V_{fc}}{2l_1} - \frac{X_3}{2l_1} - \frac{r_1 X_1}{l_1} \tag{8}$$

Eq. (9): represents the average dynamics of the UC current (X_2):

$$\dot{X}_2 = \mu_{34}\frac{(2V_{uc} + X_3)}{2l_2} - \frac{X_3}{2l_2} - \frac{r_2 X_2}{l_2} \tag{9}$$

Eq. (10): governs the average dynamics of the DC-bus voltage (X_3):

$$\dot{X}_3 = (1 - \mu_1)\frac{X_1}{2c} + (1 - \mu_{34})\frac{X_2}{2c} - \frac{i_0}{c} \tag{10}$$

Where:
- X_1 is the average FC current ($< I_{fc} >$).
- X_2 is the average UC current ($< I_{uc} >$).
- X_3 is the average voltage of the DC-bus ($< V_{dc} >$).
- μ_1 is the average duty ratio ($< \mu_1 >$).
- μ_{34} is the average duty ratio ($< \mu_{34} >$).

Modeling Assumptions: The proposed mathematical model is developed under CCM operation of the tri-state converters. State-space averaging is employed to obtain the averaged system model over one switching period. The inductor resistances r_1 and r_2 are included in the model, whereas higher-order parasitic effects are neglected. In addition, all state variables required for feedback control are assumed to be measurable. These average models provide a simplified representation of the system's behavior over one switching period, which is useful for designing a controller to regulate and optimize the system's performance. The control inputs μ_1 and μ_{34} play a crucial role in this controller design.

Journal Pre-proof

Journal Pre-proof

IV. Controller design and analysis

Unlike conventional boost and buck-boost converter topologies that suffer from non-minimum phase behavior due to the presence of RHP zero in CCM operation, the proposed tri-state converter configuration enables improved controllability and faster transient response. This feature facilitates the effective implementation of nonlinear controllers for achieving rapid DC-bus voltage regulation and robust current tracking in EV applications. In addition to controller synthesis, rigorous stability analysis based on Lyapunov theory is carried out to establish global asymptotic convergence of the closed-loop system states. This theoretical analysis provides mathematical guarantees for the stability of the system under the proposed nonlinear control framework. In this section, the paper proposes the use of Lyapunov redesign, SMC, and ST-SMC techniques to achieve the following objectives.

- Regulating the DC-bus voltage to its reference value.
- Tracking the UC current (X_2) to its nominal value.
- Performing global asymptotic stabilization of the entire system.

To regulate the DC-bus voltage (X_3) to its reference value, an indirect method is employed because of the non-minimum phase behavior of the boost converter. In this method, the input current is controlled to manage the DC-bus voltage. By regulating the input current, X_1, the DC-bus voltage can be forced to reach its reference value. There is a relationship between X_1 and X_3 as described by Eq. (11):

$$X_{1ref} = \gamma \left(\frac{X_3 i_0 - V_{uc} X_{2ref}}{V_{fc}} \right) \tag{11}$$

- γ is the ideality factor, which has a value greater than or equal to 1.

This Eq. establishes a relationship between the reference current (X_{1ref}), DC-bus voltage (X_3), output current (i_0), UC voltage (V_{uc}) and reference current (X_{2ref}). It is used as part of the control strategy to achieve the desired voltage regulation and current tracking objectives.

A. Lyapunov based control

In this section, the paper presents a control strategy using the Lyapunov redesign to achieve the following goals:

- Regulate X_3 to its reference value.
- Track X_1 to its nominal value.
- Ensure the global asymptotic stability of the entire system.

To facilitate control design, the article defines error terms for FC current (e_1), UC current (e_2), and DC bus voltage (e_3) relative to their respective reference values:
Eqs (12-14):

$$e_1 = X_1 - X_{1ref} \tag{12}$$

$$e_2 = X_2 - X_{2ref} \tag{13}$$

$$e_3 = X_3 - X_{3ref} \tag{14}$$

Here, e_1, e_2, and e_3 represent the error terms for FC current, UC current, and DC-bus voltage, respectively, with respect to their reference values. The goal is to make these error terms converge to zero for DC-bus voltage regulation and FC current tracking. To design the controller, analyze the time derivative of these error terms. For e_1, taking the derivative of Eq. (12) leads to:

$$\dot{e}_1 = \dot{X}_1 - \dot{X}_{1ref} \tag{15}$$

Substituting the expression for X_1 from Eq. (8) into Eq. (15) gives the following:

$$\dot{e}_1 = \mu_1 \frac{(V_{fc} + X_3)}{2l_1} + \frac{V_{fc}}{2l_1} - \frac{X_3}{2l_1} - \frac{r_1 X_1}{l_1} - \dot{X}_{1ref} \tag{16}$$

To achieve exponential stability for e_1, the aim is to make it behave as follows in Eq. (17):

$$\dot{e}_1 = -c_1 e_1 + e_3 \tag{17}$$

Journal Pre-proof

Journal Pre-proof

Here, $c_1 > 0$ is a positive design parameter. Rearranging Eq. (16) and equating it with the desired error dynamics in Eq. (17), the control law for μ_1 can be obtained:

$$\mu_1 = \frac{2l_1}{V_{fc} + X_3}\left(e_3 - c_1 e_1 - \frac{V_{fc}}{2l_1} + \frac{X_3}{2l_1} + \frac{r_1 X_1}{l_1} + \dot{X}_{1ref}\right) \tag{18}$$

To regulate the DC-bus voltage, a damping term e_3 is introduced in Eq. (18). The dynamics of e_3 will be analyzed later. Next, the controller signal μ_{34} for the Tri-state buck-boost converter is designed. To do this, the time derivative of e_3 is considered: Eq. (19):

$$\dot{e}_2 = \dot{X}_2 - \dot{X}_{2ref} \tag{19}$$

By substituting the expression for $\dot{X}_2$from Eq. (9) into Eq. (19), we get:

$$\dot{e}_2 = \mu_{34}\frac{(2V_{uc} + X_3)}{2l_2} - \frac{X_3}{2l_2} - \frac{r_2 X_2}{l_2} - \dot{X}_{2ref} \tag{20}$$

To ensure exponential stability for e_2, we define it as follows:

$$\dot{e}_2 = -c_2 e_2 \tag{21}$$

where $c_2 > 0$ is a positive design parameter. Similarly, comparing Eq. (20) and (21), the control input μ_{34} is derived to ensure the exponential convergence of e_2:

$$\mu_{34} = \frac{2l_2}{2V_{uc} + X_3}\left(-c_2 e_2 + \frac{X_3}{2l_2} + \frac{r_2 X_2}{l_2} + \dot{X}_{2ref}\right) \tag{22}$$

To prove global asymptotic stability, a Lyapunov function V is defined as follows:

$$V = \frac{1}{2}(e_1^2 + e_2^2 + e_3^2) \tag{23}$$

The candidate Lyapunov function V is positive definite since $V > 0$ for all nonzero error states and $V = 0$ only at the equilibrium point. Therefore, if its time derivative $\dot{V}$ is negative definite, global asymptotic stability of the closed-loop system is guaranteed according to the Lyapunov stability theory. The time derivative of V is given by:
Eq. (24):

$$\dot{V} = e_1\dot{e}_1 + e_2\dot{e}_2 + e_3\dot{e}_3 \tag{24}$$

Substituting the expressions for $\dot{e}_1$ and $\dot{e}_2$ from Eq.s (22) and (21), respectively, into Eq. (24), it becomes:
Eq. (25):

$$\dot{V} = -c_1 e_1^2 - c_2 e_2^2 + e_3(e_1 + \dot{e}_3) \tag{25}$$

The first two terms in Eq. (25) are already negative and the purpose of the paper is to make the third term negative to ensure that $\dot{V}$ is negative. To achieve this, e_3 must follow the dynamics given by Eq. (26):

$$\dot{e}_3 = -c_3 e_3 - e_1 \tag{26}$$

Here, $c_3 > 0$ is a positive design parameter. Substituting Eq. (26) into Eq. (25) eliminates the cross-coupling term $e_1 e_3$, resulting in a negative definite Lyapunov derivative.

$$\dot{V} = -c_1 e_1^2 - c_2 e_2^2 - c_3 e_3^2 \tag{27}$$

Eq. (27) demonstrates that the derivative of the candidate Lyapunov function is negative definite. Therefore, according to Lyapunov stability theory, the closed-loop system is globally asymptotically stable. This rigorous mathematical proof establishes guaranteed convergence of tracking errors and strengthens the theoretical validity of the proposed control framework beyond conventional simulation-only verification approaches.
To generate the nominal value for the DC-bus voltage (X_{3ref}), the paper takes the time derivative of Eq. (14) as shown in Eq. (28).

$$\dot{e}_3 = \dot{X}_3 - \dot{X}_{3ref} \tag{28}$$

By substituting the expression for $\dot{X}_3$ from Eq. (10) into Eq. (28), the paper derives Eq. (29).

$$\dot{e}_3 = (1 - \mu_1)\frac{X_1}{2c} + (1 - \mu_{34})\frac{X_2}{2c} - \frac{i_0}{c} - \dot{X}_{3ref} \tag{29}$$

Journal Pre-proof

$$\dot{X}_{3ref} = (1-\mu_1)\frac{X_1}{2c} + (1-\mu_{34})\frac{X_2}{2c} - \frac{i_0}{c} + e_1 + c_3 e_3 \tag{30}$$

Finally, by solving for X_{3ref} in Eq. (30), the paper obtains an expression that allows the calculation of X_{3ref} based on the values of X_1, X_2, μ_1, μ_{34}, i_0 and the error terms e_1 and e_3.

$$X_{3ref} = \frac{1}{s}\left((1-\mu_1)\frac{X_1}{2c} + (1-\mu_{34})\frac{X_2}{2c} - \frac{i_0}{c} + e_1 + c_3 e_3\right) \tag{31}$$

This completes the analysis of the Lyapunov-based control strategy for the regulation of DC-bus voltage and FC current tracking in the hybrid energy storage system.

B. Sliding mode controller design

SMC stands out as a robust nonlinear control technique, offering numerous advantages compared to traditional linear and nonlinear controllers. These advantages include a reduced steady-state error, finite-time convergence, and a straightforward design process. The SMC methodology typically unfolds in two distinctive phases: the reaching phase and the sliding phase. During the reaching phase, the control law is skillfully crafted to guide the system towards a designated sliding surface. Subsequently, in the sliding phase, the system adeptly follows this surface toward its desired equilibrium point. This process can be visually represented in the SMC phase diagram, as illustrated in Fig.4. Initially, the variable X_0 assumes an initial value and then progressively converges towards the sliding surface. Ultimately, through well-designed control actions,the desired final value is achieved. In the state-space model discussed above, there are two control inputs, μ_1 and μ_{34}. Therefore, it is

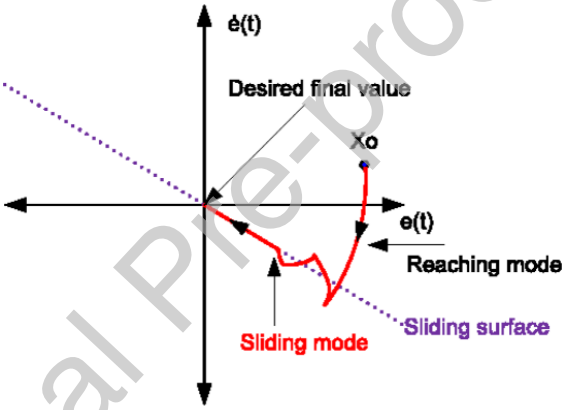


Fig. 4: Phase diagram of SMC

necessary to define two sliding surfaces as follows:

$$s_1 = c_1 e_1 \tag{32}$$

$$s_2 = c_2 e_2 \tag{33}$$

Here, c_1 and c_2 are system parameters associated with s_1 and s_2, respectively. Taking the time derivative of Eqs. (32) and (33) results in the following Eq. (34).

$$\dot{s}_1 = c_1 \dot{e}_1 \tag{34}$$

$$\dot{s}_2 = c_2 \dot{e}_2 \tag{35}$$

By substituting the expressions for $\dot{e}_1$ and $\dot{e}_2$ from Eqs. (16) and (20) into Eqs. (34) and (35), respectively.

$$\dot{s}_1 = c_1\left(\mu_1\frac{(V_{fc}+X_3)}{2l_1} + \frac{V_{fc}}{2l_1} - \frac{X_3}{2l_1} - \frac{r_1 X_1}{l_1} - \dot{X}_{1ref}\right) \tag{36}$$

$$\dot{s}_2 = c_2\left(\mu_{34}\frac{(2V_{uc}+X_3)}{2l_2} - \frac{X_3}{2l_2} - \frac{r_2 X_2}{l_2} - \dot{X}_{2ref}\right) \tag{37}$$

To achieve global asymptotic stability of the system, let us consider a positive semi-definite function $V_1 \geq 0$ as a Lyapunov candidate function:

$$V_1 = \frac{1}{2}(s_1^2 + s_2^2) \tag{38}$$

Now, by taking the time derivative of Eq. (38):

$$\dot{V}_1 = s_1\dot{s}_1 + s_2\dot{s}_2 \tag{39}$$

Journal Pre-proof

Substituting the values of $\dot{s}_1$ and $\dot{s}_2$ from Eqs. (36) and (37) into Eq. (39), we get:

$$\dot{V}_1 = s_1\left(\mu_1\frac{c_1(V_{fc}+X_3)}{2l_1}+\frac{c_1V_{fc}}{2l_1}-\frac{c_1X_3}{2l_1}-\frac{c_1r_1X_1}{l_1}-c_1\dot{X}_{1ref}\right)+s_2\left(\mu_{34}\frac{c_2(2V_{uc}+X_3)}{2l_2}-\frac{c_2X_3}{2l_2}-\frac{c_2r_2X_2}{l_2}-c_2\dot{X}_{2ref}\right) \quad (40)$$

To analyze the stability of the system using the SMC, the following constraints are used on the control inputs μ_1 and μ_{34} as given:

$$-k_1|s_1|^{\alpha}sign(\frac{s_1}{\phi_1}) = \mu_1\frac{c_1(V_{fc}+X_3)}{2l_1}+\frac{c_1V_{fc}}{2l_1}-\frac{c_1X_3}{2l_1}-\frac{c_1r_1X_1}{l_1}-c_1\dot{X}_{1ref} \quad (41)$$

$$-k_2|s_2|^{\beta}sign(\frac{s_2}{\phi_2}) = \mu_{34}\frac{c_2(2V_{uc}+X_3)}{2l_2}-\frac{c_2X_3}{2l_2}-\frac{c_2r_2X_2}{l_2}-c_2\dot{X}_{2ref} \quad (42)$$

The expressions introduced $\dot{s}_1 = -k_1|s_1|^{\alpha}sign(\frac{s_1}{\phi_1})$ and $\dot{s}_2 = -k_2|s_2|^{\beta}sign(\frac{s_2}{\phi_2})$ are referred to as hitting laws in the SMC framework. These laws play a crucial role in achieving the desired behavior of the system. They are designed as power rate reaching laws, which means that they control the rate at which the system approaches the sliding surface when the states deviate from it. The purpose of these laws is to improve reaching speed, ensuring that the system converges to the sliding surface more quickly when it moves away from it. This is a key feature of SMC as it allows for fast and robust control actions to bring the system back to the desired state.

These laws are based on the absolute values of the sliding surface variables s_1 and s_2, raised to the powers α and β, respectively, and are multiplied by appropriate signs and constants. The parameters α and β are typically chosen based on the desired response characteristics of the system, and ϕ_1 and ϕ_2 are introduced to mitigate chattering, which is a common problem in SMC.

In general, these hitting laws are a fundamental part of the SMC strategy, contributing to its robustness, finite-time convergence, and effectiveness in controlling complex systems [26].

$$sign(s_a) = \begin{cases} -1, & \text{if } s_a < 0 \\ 0, & \text{if } s_a = 0 \\ 1, & \text{if } s_a > 0 \end{cases} \quad (43)$$

After solving Eqs. (41) and (42) for the control inputs μ_1 and μ_{34}:

$$\mu_1 = \frac{2l_1}{c_1(V_{fc}+X_3)}\left(-k_1|s_1|^{\alpha}sign(\frac{s_1}{\phi_1})-\frac{c_1V_{fc}}{2l_1}+\frac{c_1X_3}{2l_1}+\frac{c_1r_1X_1}{l_1}+c_1\dot{X}_{1ref}\right) \quad (44)$$

$$\mu_{34} = \frac{2l_2}{c_2(2V_{uc}+X_3)}\left(-k_2|s_2|^{\beta}sign(\frac{s_2}{\phi_2})+\frac{c_2X_3}{2l_2}+\frac{c_2r_2X_2}{l_2}+c_2\dot{X}_{2ref}\right) \quad (45)$$

To analyze stability using Eqs. (41), (42), and (40), the time derivative of V_1 can be expressed as:

$$\dot{V}_1 = -s_1k_1|s_1|^{\alpha}sign(\frac{s_1}{\phi_1})-s_2k_2|s_2|^{\beta}sign(\frac{s_2}{\phi_2}) \le 0 \quad (46)$$

Eq. (46) demonstrates that the time derivative of the Lyapunov candidate function V_1 is definite negative, indicating that the system is globally asymptotically stable. The defined controllers meet the necessary criteria for stability analysis. Therefore, it can be concluded that the system achieves global asymptotic stability with these controllers in place.

C. Super-twisting sliding mode controller design

To mitigate the chattering phenomenon associated with traditional SMC, the ST-SMC is introduced. In the context of the control inputs μ_1 and μ_{34}, Eqs. (41) and (42) are modified as follows:

$$-k_1|s_1|^{\alpha}sign(\frac{s_1}{\phi_1})-m_1\int sign(\frac{s_1}{\phi_1})\,dt = \mu_1\frac{c_1(V_{fc}+X_3)}{2l_1}+\frac{c_1V_{fc}}{2l_1}-\frac{c_1X_3}{2l_1}-\frac{c_1r_1X_1}{l_1}-c_1\dot{X}_{1ref} \quad (47)$$

$$-k_2|s_2|^{\beta}sign(\frac{s_2}{\phi_2})-m_2\int sign(\frac{s_2}{\phi_2})\,dt = \mu_{34}\frac{c_2(2V_{uc}+X_3)}{2l_2}-\frac{c_2X_3}{2l_2}-\frac{c_2r_2X_2}{l_2}-c_2\dot{X}_{2ref} \quad (48)$$

Solving Eqs. (47) and (48) for control inputs μ_1 and μ_{34} gives the following Eqs.:

$$\mu_1 = \frac{2l_1}{c_1(V_{fc}+X_3)}\left(-k_1|s_1|^{\alpha}sign(\frac{s_1}{\phi_1})-m_1\int sign(\frac{s_1}{\phi_1})\,dt-\frac{c_1V_{fc}}{2l_1}+\frac{c_1X_3}{2l_1}+\frac{c_1r_1X_1}{l_1}+c_1\dot{X}_{1ref}\right) \quad (49)$$

$$\mu_{34} = \frac{2l_2}{c_2(2V_{uc}+X_3)}\left(-k_2|s_2|^{\beta}sign(\frac{s_2}{\phi_2})-m_2\int sign(\frac{s_2}{\phi_2})\,dt+\frac{c_2X_3}{2l_2}+\frac{c_2r_2X_2}{l_2}+c_2\dot{X}_{2ref}\right) \quad (50)$$

Journal Pre-proof

Journal Pre-proof

For stability analysis, considering Eqs. (47), (48), and (40), the candidate Lyapunov function $\dot{V}_1$ takes the following form:

$$\dot{V}_1 = -s_1 k_1 |s_1|^{\alpha} sign(\frac{s_1}{\phi_1}) - s_1 m_1 \int sign(\frac{s_1}{\phi_1})\, dt - s_2 k_2 |s_2|^{\beta} sign(\frac{s_2}{\phi_2}) - s_2 m_2 \int sign(\frac{s_2}{\phi_2})\, dt \leq 0 \tag{51}$$

The negative definiteness of $\dot{V}_1$ demonstrates that the system is globally asymptotically stable. This modification of the control laws effectively reduces chattering, making the control approach more robust and practical for real-world applications.

V. Simulation result

In this section, simulations have been performed to evaluate the performance of the designed controllers based on Eqs. (18), (22), (44), (45), (49), and (50). The model is evaluated using MATLAB/Simulink. The simulations were carried out in MATLAB/Simulink 2021b using the auto- (automatic solver selection) variable-step solver. The solver configuration and sampling rates were selected as automatic to ensure numerical stability and accurate representation of the fast switching dynamics of the proposed converters. The simulation was also tested with a fixed step automatic solver with fixed step size (fundamental sample time) of $0.00001s$. Different load variations are considered to assess the effectiveness of the controllers. The primary objective of these controllers is to regulate the DC-bus voltage to its reference value and monitor the current flow while generating nominal values for the power sources. The simulation parameters used in this work have been sourced from [32]. Table I provides the nominal parameters of the power sources, while Table II lists the parameters relevant to the DC-DC power converters used in this study. Table III outlines the parameters specific to the FHEV.
The design parameters for the Lyapunov redesign, the SMC, and the ST-SMC can be found in Table IV, selected through an iterative tuning procedure based on stability constraints, transient response requirements, and disturbance rejection performance.
Figs. 5 and 6 show the tracking of FC and UC currents, respectively. Both sources accurately track their respective references.

TABLE I: Parameters of power sources

Component	Specification
PEMFC	$200V$, $180A$, $36KW$
UC Module	$200V$, $1.66mF$

TABLE II: Parameters of DC-DC power converter

Parameter	Values
Inductors L_1 and L_2	$3300\mu H$
Inductor Resistances R_1 and R_2	$0.0022ohm$
Output Capacitance C_0	$1660\mu F$
λ	1.209

TABLE III: Parameters specifications for FHEV

Parameter	Values
car Mass M	$1066Kg$
Passenger Weight ($X2$)	$70 + 70Kg$
Aerodynamic drag coefficient C_x	0.19
Rolling resistance coefficient C_r	$1.8m^2$
Switching frequency	$100KHz$

TABLE IV: Design parameters for Lyapunov, SMC, and ST-SMC

Model	k1	k2	a1	a2	m1	m2
Lyapunov	10000	100000	–	–	–	–
SMC	3000	3000	1	1	–	–
ST-SMC	300	3000	0.01	1	0.1	1

The FC exhibits positive current tracking, as intended, while the UC demonstrates both positive and negative current tracking. This flexibility is essential for scenarios where the UC alternates between charging and discharging modes based on load conditions.
In situations with low load conditions, the UC operates in charging mode, while the FC supplies the load. In contrast, during high-load conditions, the UC switches to discharging mode. These results demonstrate the effectiveness of the proposed controllers in achieving precise current tracking for both power sources, thus optimizing the energy management system.

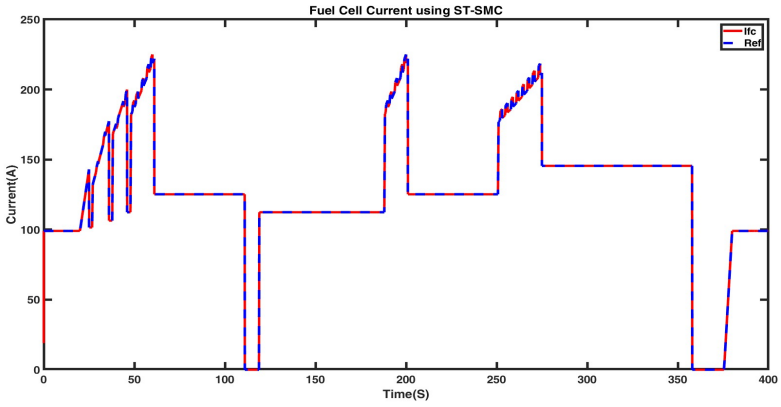


Fig. 5: Response of Fuel cell current (EUDC) for ST-SMC

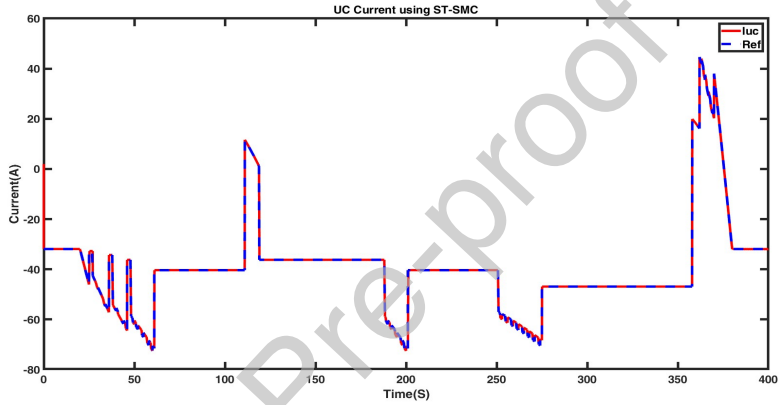


Fig. 6: Response of UC current (EUDC) for ST-SMC

A. *European Extra Urban Driving Test (EUDC) test*

The performance of the controllers has been evaluated using the European Extra Urban Driving Test (EUDC), which simulates real-world driving scenarios, including vehicle starts, constant loads, and varying load accelerations. Fig.7 shows the vehicle speed in kilometers per hour (Km/hr), while Fig.8 shows the vehicle's load current during the EUDC test. The load current varies on the basis of the vehicle's speed, with higher speeds corresponding to maximum load current and lower speeds resulting in minimum load current.
To calculate the load current (i_{load}), the following formula is used:

$$P_{out} = \frac{1}{0.75}\left(0.5P_aV_t^2AC_X + MgC_r + M\frac{dv_t}{dt}\right)v_t \tag{52}$$

$$i_{load} = \frac{1}{(0.75)(400)}\left(0.5P_aV_t^2AC_X + MgC_r + M\frac{dv_t}{dt}\right)v_t \tag{53}$$

Here, v_t represents the speed of the vehicle, A is the front area of the vehicle, M is the mass of the vehicle, C_r is the coefficient of resistance to rolling, p_a is the density of air, and C_x is the drag coefficient for aerodynamics.
These figures and calculations help assess how well the controllers manage the vehicle's power sources under various driving conditions, demonstrating their effectiveness in practical scenarios.

B. *Testifying robustness of ST-SMC*

One of the primary objectives of using ST-SMC is to achieve robustness to disturbances. To assess whether ST-SMC exhibits robustness to disturbances, let us introduce a disturbance into one of the system dynamics.
Fig.9 illustrates the disturbance, which ranges from -500 to 500 units. Fig.10 shows the response of the DC-bus voltage to this disturbance when using ST-SMC. A closer look at the zoomed-in view of Fig.10 reveals that ST-SMC responds exceptionally

Journal Pre-proof

Journal Pre-proof

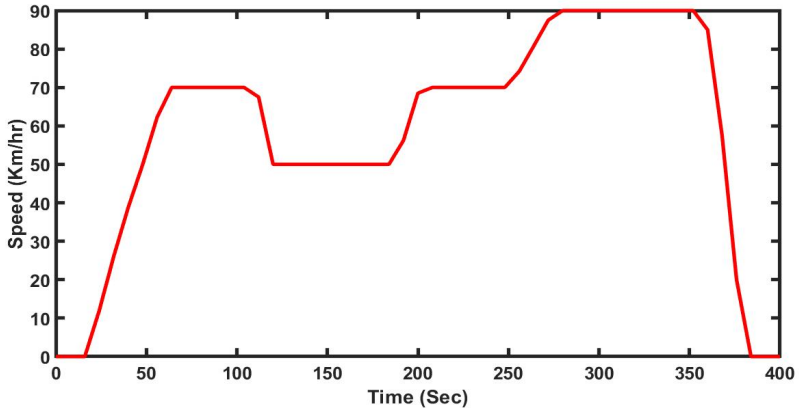


Fig. 7: Vehicle speed profile (EUDC)

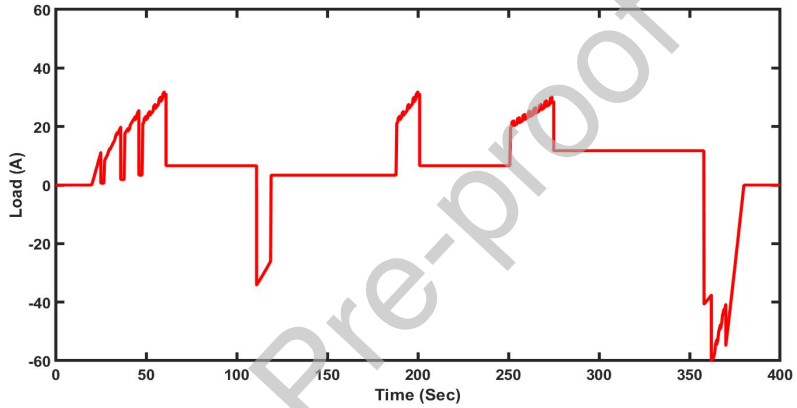


Fig. 8: Load current profile (EUDC)

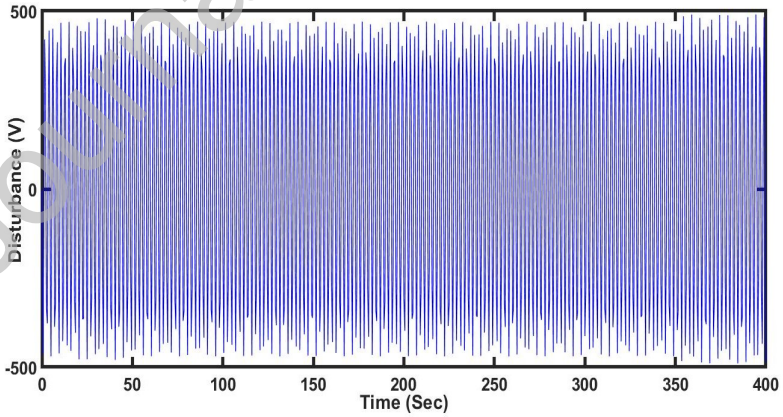


Fig. 9: Disturbance signal used for robustness evaluation

well to the disturbance. Only a minor variation of 0.3 volts is observed in response to a disturbance of 500 units.
Figs.11 and 12 depict the error between the FC current and its reference value and the UC current and its reference value, respectively. Furthermore, Figs.13 and 14 show the duty ratios (μ_1 and μ_{34}) employed by ST-SMC when subjected to disturbance.
These results demonstrate the robustness of ST-SMC, as it effectively maintains stable operation even in the presence of significant disturbances.

Journal Pre-proof

Journal Pre-proof

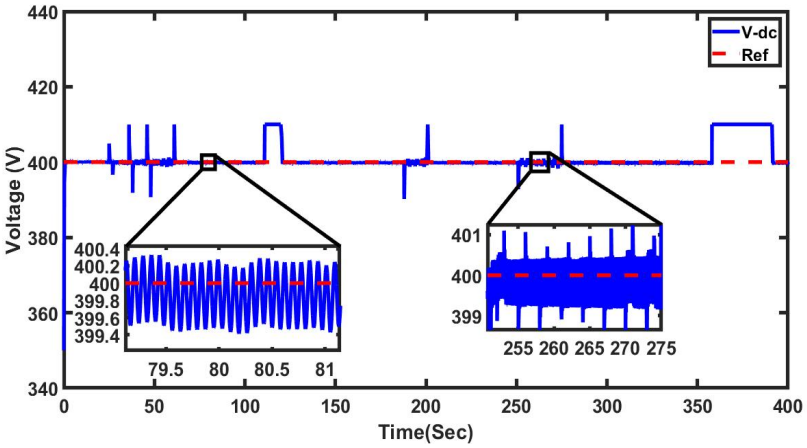


Fig. 10: Response of DC-bus voltage(EUDC) with disturbance using ST-SMC

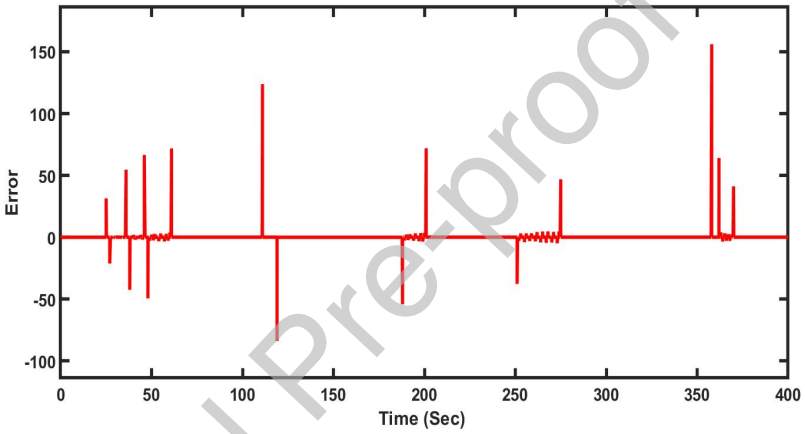


Fig. 11: Error between FC to its reference using ST-SMC

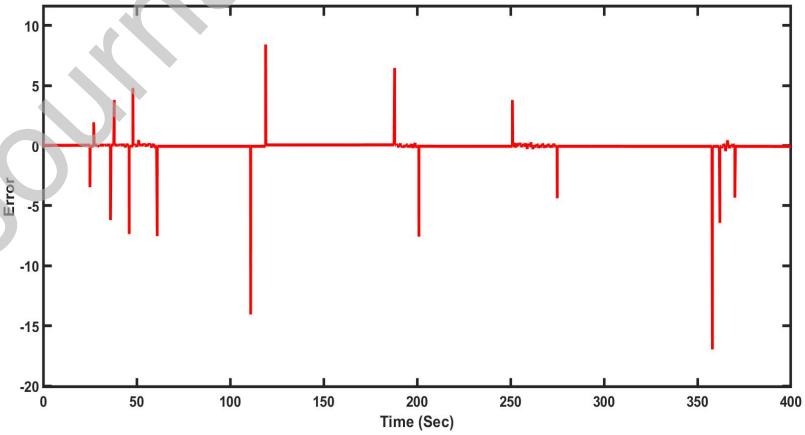


Fig. 12: Error between UC to its reference using ST-SMC

C. Comparison among Lyapunov redesign, SMC, and ST-SMC

In Fig.17, the feedback for the DC bus voltage is shown using the Lyapunov redesign, the SMC and the ST-SMC controller. The Lyapunov redesign controller has some undershoots and overshoots, which can be attributed to load current variations. To mitigate these tracking errors, overshoots, and undershoots, an SMC approach is introduced. In particular, SMC provides improved results compared to the Lyapunov redesign. To further enhance DC-bus voltage regulation and minimize undershoots and overshoots, ST-SMC is proposed. This controller demonstrates nearly zero tracking error and significantly

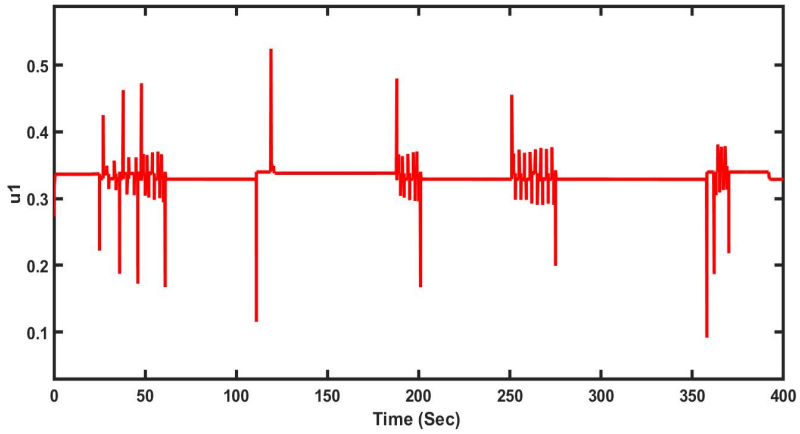


Fig. 13: Duty ratio u1 for ST-SMC (EUDC)

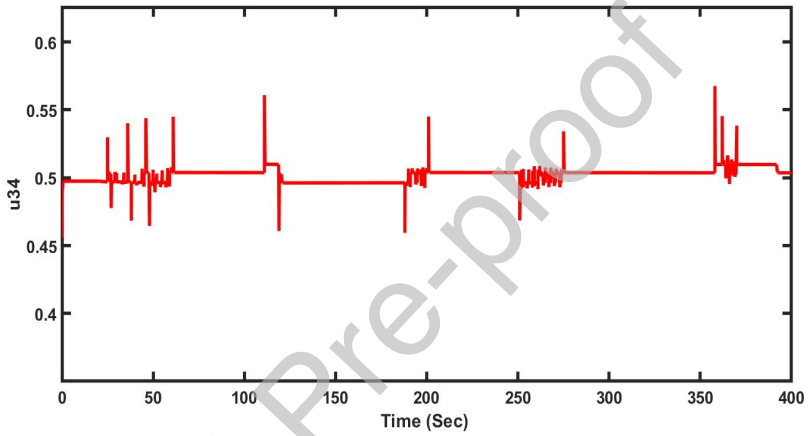


Fig. 14: Duty ratio u34 of ST-SMC (EUDC)

reduces overshoots and undershoots. It is evident that ST-SMC outperforms the other two controllers. Compared with the Lyapunov redesign and conventional SMC approaches, the ST-SMC achieves a lower steady-state error, faster convergence, and significantly reduced voltage overshoot and undershoot. In addition, the chattering phenomenon observed in conventional SMC is substantially mitigated through the super-twisting algorithm, as presented in Table V.

Fig.15 compares the FC current tracking performance among Lyapunov Redesign, SMC, and ST-SMC. Fig.16 illustrates

TABLE V: Comparative assessment of Lyapunov, SMC, and ST-SMC

Controller	Settling time	Steady-State Error	Overshoot	Ripple	Chattering	Robustness
Lyapunov	$0.3s$	$4v$	Maximum	High	No	Weak
SMC	$0.25s$	$0.3v$	Medium	Medium	High	Strong
ST-SMC	$0.2s$	$0.05v$	Low	Low	Very Low	Very Strong

TABLE VI: Comparative ISE Analysis of the Designed Controllers Using the Proposed Model

Controllers	Driving test	ISE
ST-SMC	EDUC	1.689×10^4
SMC	EDUC	1.710×10^4
Lyapunov	EDUC	1.794×10^4

the current tracking performance of the UC for the three controllers. Fig.17 shows a comparison of the DC bus voltage for Lyapunov Redesign, SMC, and ST-SMC.

Upon close examination of these zoomed-in view figures, it becomes evident that ST-SMC outperforms the other two controllers. It exhibits nearly zero tracking error with minimal undershoot and overshoot in the DC-bus voltage. This comparison highlights the superior performance of ST-SMC in terms of tracking accuracy and stability.

Fig. 18 , represents the voltage of the DC bus for conventional and Tri-State power converters with the same parametric data.

Journal Pre-proof

TABLE VII: Comparative ISE Analysis using conventional Boost and Buck-Boost Converters

	Controllers	Driving test	ISE
[34]	PI	EDUC	1.2773×10^7
	SMC	EDUC	1.663×10^6
	ISMC	EDUC	1.116×10^6
	DISMC	EDUC	1.043×10^6

One can clearly see that the conventional converter has an initial undershoot while the Tri-state has no initial undershoot in the voltage. The tri-state converter exhibits a faster transient response and a lower settling time than the conventional converter. Table VI contains the Integration of square error (ISE) for the proposed model while table VII represents ISE for the conventional model proposed in [34]. These results demonstrate the superior dynamic performance of the proposed tri-state converter compared with conventional converter topologies.

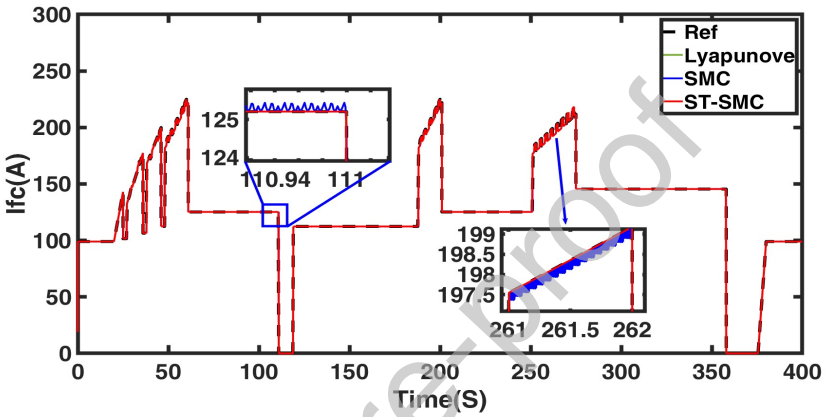


Fig. 15: Comparison graph of FC current among Lyapunov redesign, SMC, and ST-SMC

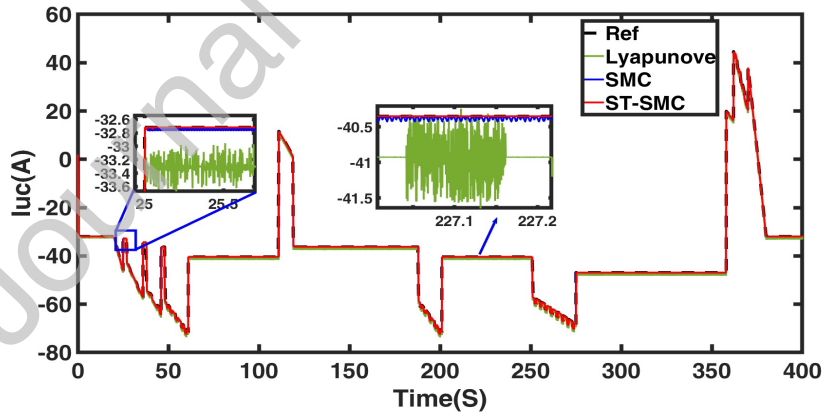


Fig. 16: Comparison graph of UC current among Lyapunov redesign, SMC, and ST-SMC

D. Testifying Hardware-in-loop

In the HIL experiment, the dynamic model implemented in Simulink is validated through real-time analysis. This process is essential before practical implementation. The HIL set-up consists of both software and hardware components, as depicted in Fig.19. The hardware setup comprises a host computer and an MCU F28379D Dual Core $Delfino^{TM}$ microcontroller. The microcontroller is responsible for executing the duty ratios μ_1 and μ_{34}, connected to MATLAB through the $TIC2000$ Delfino platform, which facilitates the communication between the microcontroller and MATLAB. On the software side of the setup, a dynamic block is executed within MATLAB/Simulink. This approach simplifies the system's complexity and allows for the validation of the dynamic model using real-time hardware. The entire process involves several stages. Initially, the plant model or HESS (discrete version) is translated into MATLAB/Simulink compatible code with the following solver details:

Journal Pre-proof

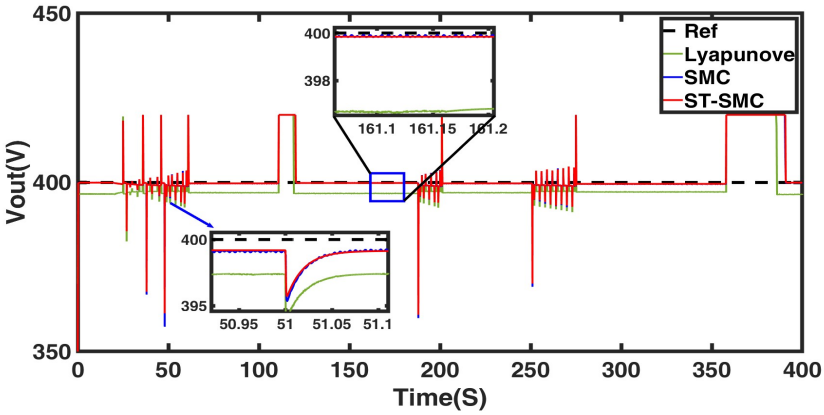


Fig. 17: Comparison graph of DC-bus voltage among Lyapunov redesign, SMC and ST-SMC

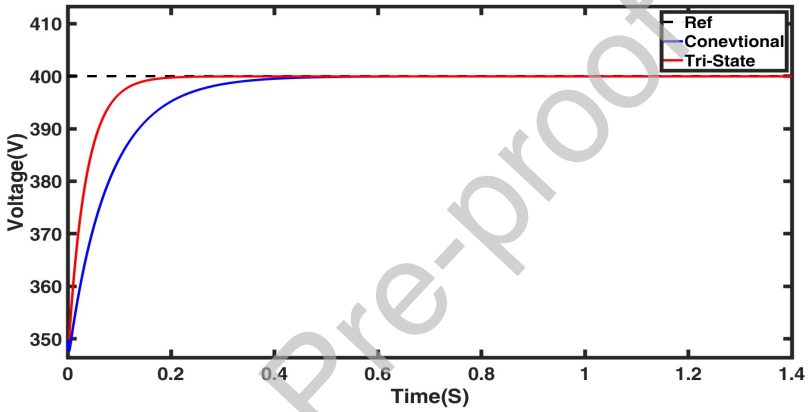


Fig. 18: DC bus voltage comparison graph of ST-SMC between Tri-State and Conventional Converters

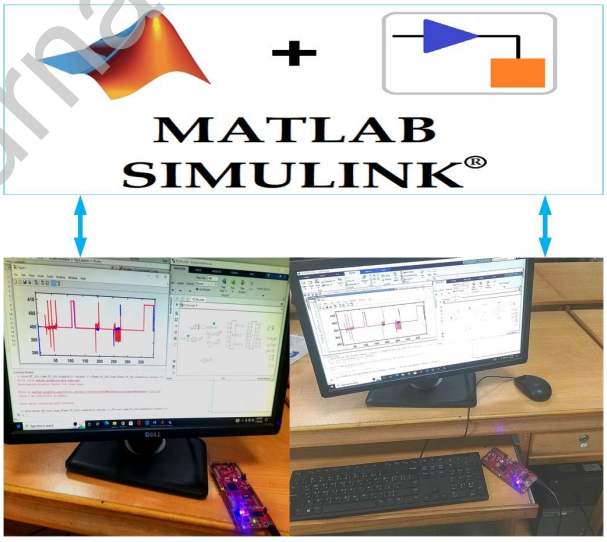


Fig. 19: HIL setup

fixed-step discrete time solver with fixed-step size (fundamental sample time) of 0.00001s. The HIL simulation starts after around 10s, as shown in HIL figures. In the second stage, this code is loaded onto the micro-controller with the assistance of the host computer to generate Pulse Width Modulation (PWM) signals. These PWM signals are used for the switching operations within the system. In the final stage, the desired figures, such as FC current, UC current, and DC-bus voltage, are

Journal Pre-proof

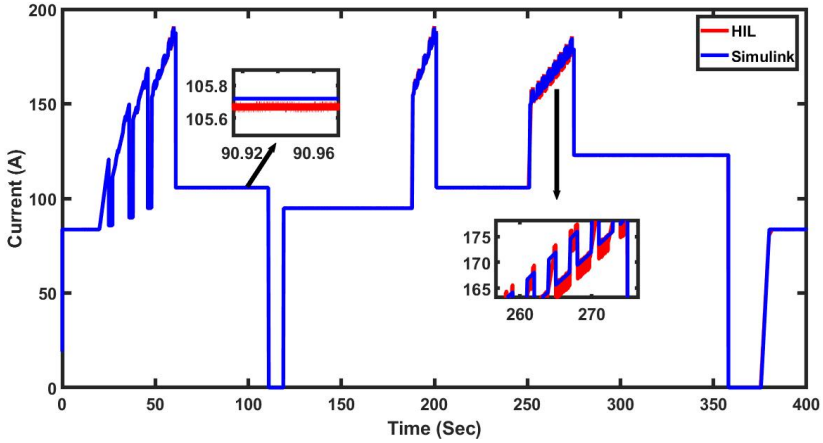


Fig. 20: Comparison graph of HIL and simulation of FC current using ST-SMC

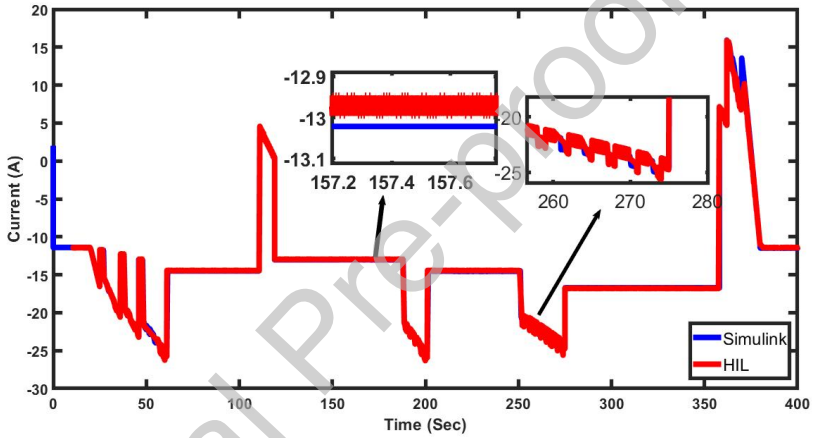


Fig. 21: Comparison graph of HIL and Simulation of UC current using ST-SMC

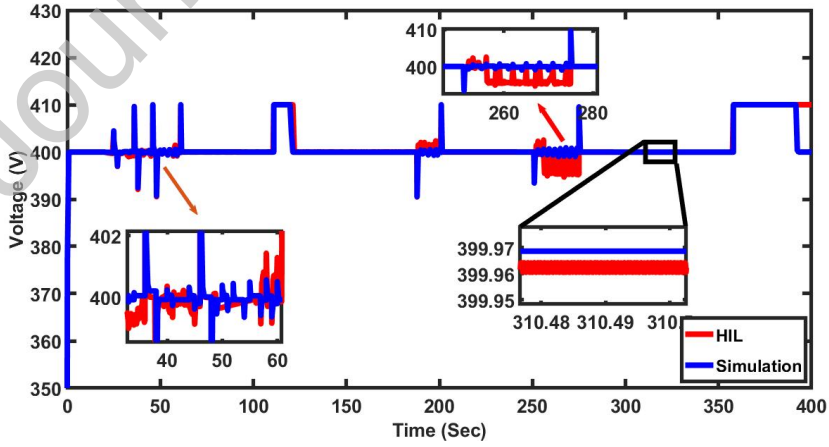


Fig. 22: Comparison graph of HIL and Simulation of DC-bus voltage using ST-SMC

displayed on the screen.

Figs.20, 21, and 22 illustrate the comparison between HIL and simulation results for FC current, UC current, and DC-bus voltage, respectively. The maximum deviation between simulation and HIL results remained below 0.1% for the DC-bus

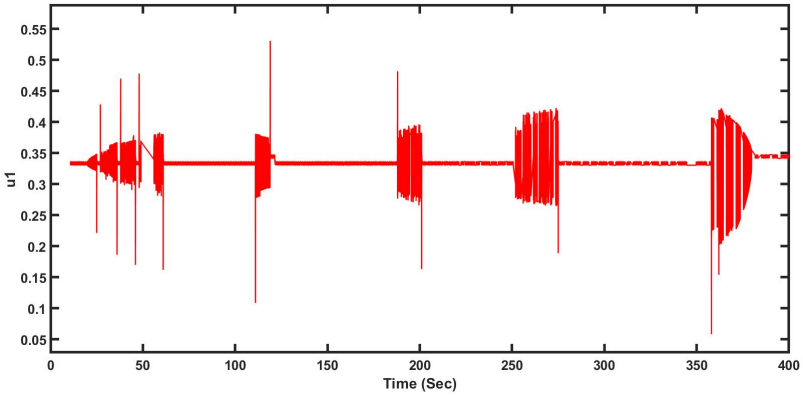


Fig. 23: Duty ratio u1 for FC using HIL (EUDC)

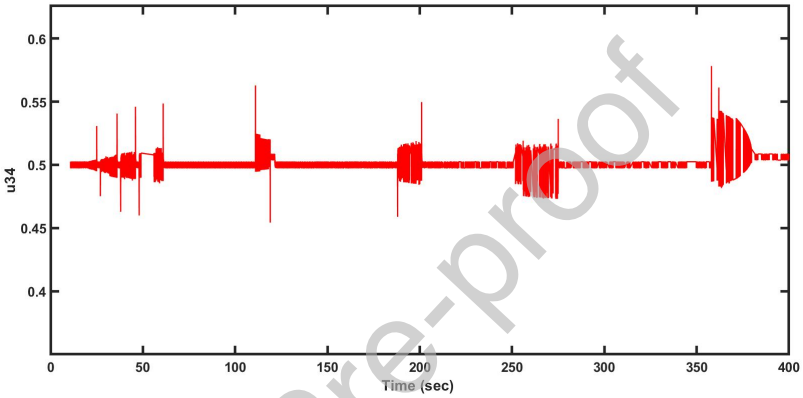


Fig. 24: Duty ratio u34 for UC using HIL (EUDC)

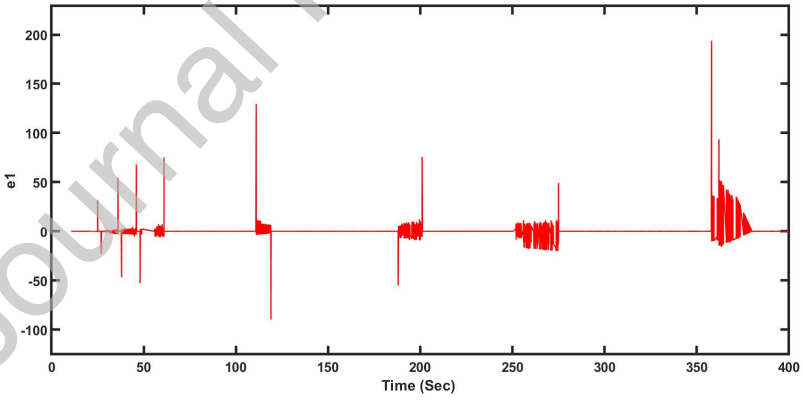


Fig. 25: Error between FC current to its reference using HIL (EUDC)

Journal Pre-proof

voltage as well as for current tracking responses, confirming a strong agreement between both implementations, indicating the effectiveness of control strategies. The close agreement between simulation and HIL results confirms the practical feasibility, real-time implementation ability, and robustness of the proposed ST-SMC approach for EV powertrain applications.
Figs.23 and 24 show the duty ratios obtained through HIL, while the error terms between X_1 and its reference, as well as X_2 and its reference, are presented in Figs.25 and 26, respectively. These results further validate the performance of the control system in a real-time hardware setup.

VI. Conclusion and Future Work

In this research study, we have undertaken the modeling and design of robust nonlinear controllers for a HESS in FC-UC based HEVs. The controllers were designed for use with Tri-state boost and Tri-state buck-boost power converters. Our investigation involved extensive simulation using MATLAB/Simulink. The controllers were rigorously evaluated under the EUDC test, which

Journal Pre-proof

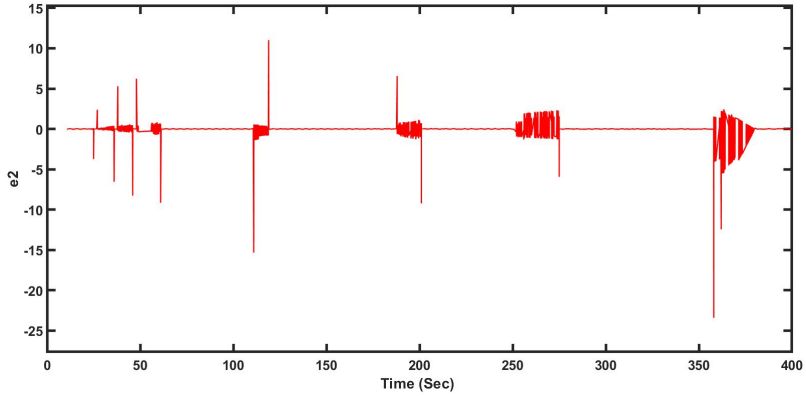


Fig. 26: Error between UC current to its reference using HIL (EUDC)

simulates real-world driving conditions that various scenarios such as vehicle start-up, steady-state operation, and changes in load acceleration. Throughout the simulations, the controllers demonstrated their ability to effectively regulate the DC-bus voltage (X_3), the FC current (X_1), and the UC current (X_2), achieving close tracking of these parameters to their respective reference values. Furthermore, the controllers exhibited reduced tracking errors and minimal overshoots in the DC-bus voltage. Among the controllers tested, the ST-SMC emerged as the top performing option, producing the most favorable results. The stability analysis is established using Lyapunov theory, affirming the global asymptotic stability of the closed-loop system.
To further validate the robustness and applicability of controllers in the real world, a HIL experiment is conducted. This experiment confirmed that the controllers maintained their performance in a real-time hardware setup. The close agreement between simulation and HIL results confirms the practical feasibility, real-time implementation ability, and robustness of the proposed ST-SMC approach for EV powertrain applications.
In conclusion, our research has successfully designed and evaluated robust nonlinear controllers for an FC-UC based HESS in an HEV. The controllers have shown their effectiveness in regulating key parameters under various driving conditions, and the ST-SMC has shown exceptional performance. These findings contribute to the advancement of control strategies for hybrid electric vehicles, potentially improving their efficiency and reliability.
A key contribution of this work is the improved transient performance as a result of a fast dynamics of the Tri-state power converters which is essential for achieving the abrupt step-up and step-down voltage changes required for EVs. Furthermore, the rigorous Lyapunov-based stability analysis distinguishes this work from purely simulation-oriented studies by providing theoretical guarantees for global asymptotic stability of the closed-loop system.

Future research will focus on sensitivity analysis of controller parameters and extending the proposed control framework to more advanced EV applications and operating conditions. In particular, the proposed controllers will be evaluated under aggressive driving cycles such as WLTP and US06 to further investigate their robustness under highly dynamic conditions. Future studies will also incorporate component aging effects, thermal variations, PEMFC degradation, and UC parameter drift into the system model to assess long-term reliability and controller robustness. Furthermore, practical considerations including optimal sizing, system weight, volumetric constraints, and techno-economic analysis of the FC–UC combination will be investigated. Furthermore, the proposed framework will be extended to emerging electrified transportation sectors, including maritime and aviation propulsion systems, while also investigating the grid-level impacts of large-scale EV adoption, such as smart energy management and vehicle-to-grid (V2G) integration [35], [36].

ACKNOWLEDGEMENT

The authors would also like to acknowledge the support of the Interdisciplinary Research Center for Sustainable Energy Systems (IRC-SES) at KFUPM, Saudi Arabia, under Project No. INSE2618.

CREDIT AUTHORSHIP CONTRIBUTION STATEMENT

Adnan Khan: Writing – original draft, Visualization, Software, Methodology, Conceptualization. **Iftikhar Ahmad and Shahzad Ahmed:** Writing – original draft, Visualization, Validation, Software, Methodology, Formal analysis, Conceptualization. **Khaled S. Alatawi and Fahad M. Almasoudi:** Writing – review & editing, Visualization, Validation, Methodology, Conceptualization. **Kamran Zeb:** Writing – review & editing, Resources, Investigation, Formal analysis, Conceptualization. **Husam A. Neamah:** Writing – review & editing, Validation, Supervision, Resources, Investigation, Formal analysis, Conceptualization.

Journal Pre-proof

AUTHOR STATEMENT

This work is stated to be an original and new contribution. It has neither been sent anywhere else (conference/journal) nor it has already been published anywhere else (conference/journal).

DECLARATION OF GENERATIVE AI AND AI-ASSISTED TECHNOLOGIES IN THE WRITING PROCESS

The authors affirm that all language and content in this publication were generated without the use of AI techniques.

DECELERATION OF COMPETITOR INTEREST

We declare that we have no conflict of interest with respect to the publication of this research paper.

DATA AVAILABILITY

Data will be made available on request.

REFERENCES

[1] A. Alsinai, A. U. Khan Niazi, R. Arooj, A. Smerat, and A. A. Zaky, "Finite-time adaptive super-twisting sliding mode control of nonlinear off-road electric vehicles with terrain-induced disturbances," *Results in Engineering*, p. 109906, 2026.

[2] "Fast integral terminal sliding mode control of a multisource hybrid energy storage system in extended-range electric vehicles," *Chaos, Solitons Fractals*, vol. 209, p. 118426, 2026.

[3] R. Venkatasatish and C. Dhanamjayulu, "Reinforcement learning based energy management systems and hydrogen refuelling stations for fuel cell electric vehicles: An overview," *International Journal of Hydrogen Energy*, 2022.

[4] J. Shaik and S. Karri, "Accelerated primal–dual deep reinforcement learning for efficient energy management of hybrid electric vehicles," *Arabian Journal for Science and Engineering*, vol. 50, pp. 5525–5540, 2025. [Online]. Available: https://doi.org/10.1007/s13369-024-09353-3

[5] K. Zeb, M. Zaery, W. Uddin, M. A. Ayaz, I. Khan, M. A. Abido, and M. Khalid, "Robust super-twisting sliding mode control for ifoc-based im drive in multisource evs," in *2026 IEEE Texas Power and Energy Conference (TPEC)*, 2026, pp. 1–6.

[6] H. Aouzellag, B. Amrouche, K. Iffouzar, and D. Aouzellag, "Proposed hysteresis energy management strategy based on storage system efficiency for hybrid electric vehicle," *Journal of Energy Storage*, vol. 54, p. 105259, 2022.

[7] N. Singh, S. Tanwar, A. Sharma, and B. Yadav, "Advanced cyclic stability and highly efficient different shaped carbonaceous nanostructured electrodes for solid-state energy storage devices," *International Journal of Hydrogen Energy*, 2022.

[8] M. Kandidayeni, J. Trovão, M. Soleymani, and L. Boulon, "Towards health-aware energy management strategies in fuel cell hybrid electric vehicles: A review," *International Journal of Hydrogen Energy*, 2022.

[9] D. Kumar, R. K. Nema, and S. Gupta, "A comparative review on power conversion topologies and energy storage system for electric vehicles," *International Journal of Energy Research*, vol. 44, no. 10, pp. 7863–7885, 2020.

[10] B. Samia, A. Toufik, and H. Kamel-Eddine, "Frequency splitting approach using wavelet for energy management strategies in fuel cell ultra-capacitor hybrid system," *Journal of Measurements in Engineering*, vol. 10, no. 1, pp. 15–26, 2022.

[11] H.-B. Yuan, W.-J. Zou, S. Jung, and Y.-B. Kim, "Optimized rule-based energy management for a polymer electrolyte membrane fuel cell/battery hybrid power system using a genetic algorithm," *International Journal of Hydrogen Energy*, vol. 47, no. 12, pp. 7932–7948, 2022.

[12] N. Barhoumi, H. Marzougui, F. Bacha, and M. Boukhnifer, "Energy management algorithm of fuel cell/supercapacitor system for electrical vehicle," in *2022 8th International Conference on Control, Decision and Information Technologies (CoDIT)*, vol. 1. IEEE, 2022, pp. 1415–1420.

[13] M. S. Khan, I. Ahmad, H. Armaghan, and N. Ali, "Backstepping sliding mode control of fc-uc based hybrid electric vehicle," *IEEE Access*, vol. 6, pp. 77 202–77 211, 2018.

[14] R. S. Sankarkumar and R. Natarajan, "Energy management techniques and topologies suitable for hybrid energy storage system powered electric vehicles: An overview," *International Transactions on Electrical Energy Systems*, vol. 31, no. 4, p. e12819, 2021.

[15] T. Teng, X. Zhang, H. Dong, and Q. Xue, "A comprehensive review of energy management optimization strategies for fuel cell passenger vehicle," *International Journal of Hydrogen Energy*, vol. 45, no. 39, pp. 20 293–20 303, 2020.

[16] K. V. Singh, H. O. Bansal, and D. Singh, "Feed-forward modeling and real-time implementation of an intelligent fuzzy logic-based energy management strategy in a series–parallel hybrid electric vehicle to improve fuel economy," *Electrical Engineering*, vol. 102, no. 2, pp. 967–987, 2020.

[17] M. S. Wasim, S. Habib, M. Amjad, A. R. Bhatti, E. M. Ahmed, and M. A. Qureshi, "Battery-ultracapacitor hybrid energy storage system to increase battery life under pulse loads," *IEEE Access*, vol. 10, pp. 62 173–62 182, 2022.

[18] F. Noor, K. Zeb, S. Ullah, Z. Ullah, M. Khalid, and A. Al-Durra, "Design and validation of adaptive barrier function sliding mode controller for a novel multisource hybrid energy storage system based electric vehicle," vol. 12, 2024, pp. 145 270–145 285.

[19] A. Al-Sabaawi, K. Al-Dulaimi, E. Foo, and M. Alazab, "Addressing malware attacks on connected and autonomous vehicles: recent techniques and challenges," in *Malware Analysis Using Artificial Intelligence and Deep Learning*. Springer, 2021, pp. 97–119.

[20] X. Liu, C. Jia, and J. Ping, "Adjustable predefined time sliding mode control method for nonlinear systems with unknown disturbances," *Chaos, Solitons & Fractals*, vol. 199, p. 116667, 2025.

[21] I. Seto, S. Otaka, H. Yoshida, K. Nonin, M. Nishikawa, T. Kato, Y. Nito, H. Ishiwata, and T. Otsuki, "Sub-ghz two-way ranging based on phase detection for remote keyless entry systems," *IEEE Transactions on Vehicular Technology*, 2022.

[22] S. Ullah, R. Hayat, K. Zeb, A. Rasheed, and S. Muyeen, "Super-twisting sliding mode controller for energy storage system of a novel multisource hybrid electric vehicle: Simulation and hardware validation," *International Journal of Hydrogen Energy*, vol. 71, pp. 952–963, 2024.

[23] M. S. Khan, I. Ahmad, and F. Z. U. Abideen, "Output voltage regulation of fc-uc based hybrid electric vehicle using integral backstepping control," *IEEE Access*, vol. 7, pp. 65 693–65 702, 2019.

[24] D. Xu, Q. Liu, W. Yan, and W. Yang, "Adaptive terminal sliding mode control for hybrid energy storage systems of fuel cell, battery and supercapacitor," *Ieee Access*, vol. 7, pp. 29 295–29 303, 2019.

[25] L. Yin and Z. Su, "Multi-step depth model predictive control for photovoltaic power systems based on maximum power point tracking techniques," *International Journal of Electrical Power & Energy Systems*, vol. 131, p. 107075, 2021.

[26] G. Rojas-Dueñas, J. R. Riba, and M. Moreno-Eguilaz, "Modeling of a dc-dc bidirectional converter used in mild hybrid electric vehicles from measurements," *Measurement*, vol. 183, p. 109838, 2021.

[27] M. Anbarasi, R. Latha, and S. Adharsh Babu, "Artificial neural network controlled multi-device interleaved dc-dc boost converter implementation for electric vehicle applications," *IEEJ Transactions on Electrical and Electronic Engineering*, 2022.

[28] S. Yahyazadeh, M. Khaleghi, S. Farzamkia, and A. Khoshkbar-Sadigh, "A new structure of bidirectional dc-dc converter for electric vehicle applications," in *2020 11th Power Electronics, Drive Systems, and Technologies Conference (PEDSTC)*. IEEE, 2020, pp. 1–6.

Journal Pre-proof

[29] A. U. Rahman, S. S. Zehra, I. Ahmad, and H. Armghan, "Fuzzy supertwisting sliding mode-based energy management and control of hybrid energy storage system in electric vehicle considering fuel economy," *Journal of Energy Storage*, vol. 37, p. 102468, 2021.
[30] B. Mallikarjuna Reddy and P. Samuel, "Analysis, modelling and implementation of multi-phase single-leg dc/dc converter for fuel cell hybrid electric vehicles," *International Journal of Modelling and Simulation*, vol. 40, no. 4, pp. 279–290, 2020.
[31] K. Li, S.-C. Tan, and S. Y. R. Hui, "Dynamic response and stability margin improvement of wireless power receiver systems via right-half-plane zero elimination," *IEEE Transactions on Power Electronics*, vol. 36, no. 10, pp. 11 196–11 207, 2021.
[32] A. Goudarzian, A. Khosravi, and H. A. Raeisi, "Modeling, design and control of a modified flyback converter with ability of right-half-plane zero alleviation in continuous conduction mode," *Engineering Science and Technology, an International Journal*, vol. 26, p. 101007, 2022.
[33] N. Rana, A. Ghosh, and S. Banerjee, "Design and implementation of an improved tri-state boost converter with optimal type-iii controller," *International Journal of Power Electronics*, vol. 10, no. 3, pp. 236–265, 2019.
[34] A. U. Rahman, I. Ahmad, and A. S. Malik, "Variable structure-based control of fuel cell-supercapacitor-battery based hybrid electric vehicle," *Journal of Energy Storage*, vol. 29, p. 101365, 2020.
[35] G. Amann, V. R. Escobedo Berm'udez, E. Boskov-Kovacs, S. Gallego Amores, S. Giannelos, A. Iliceto, A. Ilo, J. R. Chavarro, N. Samovich, L. Schmitt *et al.*, "E-mobility deployment and impact on grids: impact of ev and charging infrastructure on european td grids: innovation needs," 2022.
[36] S. Giannelos, I. Konstantelos, and G. Strbac, "Optimal supply chain design using machine learning, risk assessment and optimisation applied to coal distribution," *EURO Journal on Decision Processes*, p. 100062, 2025.

Journal Pre-proof